Eur. Phys. J. D **6**, 99–108 (1999)

THE EUROPEAN PHYSICAL JOURNAL D

EDP Sciences

Calculations of structures and vibrational spectra of homogeneous and mixed SF_6 clusters with Ar

T.A. Beu[a], Y. Okada and K. Takeuchi

The Institute of Physical and Chemical Research (RIKEN), Wako-shi, 351-01 Saitama, Japan

Received: 15 September 1998 / Received in final form: 2 November 1998

Abstract. A recently reported intermolecular potential for SF_6, featuring exchange, dispersion, and electrostatic terms, is used to determine minimum energy structures of homogeneous SF_6 clusters up to the decamer. By adding appropriate interaction terms, also structures of mixed $(SF_6)_2$-Ar_n clusters are calculated. A second order line shift formalism, treating the anharmonic intramolecular force field and the intermolecular potential as a perturbation, is employed to calculate the corresponding IR-spectra in the region of the ν_3 vibrational mode of the monomer (at 947.968 cm^{-1}). The leading interaction mechanism responsible for the line shifts is confirmed to be the resonant dipole-dipole coupling. The theoretical spectra fairly describe both size-selected spectra for clusters up to the tetramer and recently measured FT-IR spectra in a continuous supersonic Laval nozzle flow.

PACS. 36.40.Mr Spectroscopy and geometrical structure of clusters

1 Introduction

Over the last two decades quite a great deal of experimental and theoretical work has been devoted to the investigation of SF_6 clusters [1–10]. The particular interest in the ν_3 vibrational mode of the monomer ($\nu_3 = 947.968$ cm^{-1}) has been, obviously, a consequence of the similarities between SF_6 and the more challenging UF_6 system, for which this mode plays a key role in the molecular laser isotope separation technique.

The ν_3 vibrational mode of SF_6 can be excited in IR predissociation experiments [1–4]. The mutual interaction of the molecules within the clusters cause the spectral bands to appear split and shifted with respect to the monomer absorption frequencies. In their measurements on SF_6 clusters, Huisken *et al.* [3] have used the size-selection technique introduced by Buck and Meyer [11], which is based on the deflection of the molecular beam by scattering from a secondary noble gas beam. To improve the spectral resolution, Heijmen *et al.* [4] have performed two-laser experiments, in which a fixed-frequency probe laser was used to label cluster levels for a certain cluster species, while the pump laser was scanned to identify IR-predissociation frequencies connected with the labeled cluster states.

Gough, Knight and Scoles observed in infrared photodepletion spectroscopy of molecular beams of SF_6-Ar_n clusters the redshifting and broadening of the ν_3 band of SF_6 [5,6]. The Monte Carlo simulations of Eichenauer and Le Roy [7] reproduced semiquantitatively the experimental spectra and showed that the broadening can be caused by phase coexistence. Extensive infrared spectroscopy studies of small solvated molecules (among others, of SF_6, too) seeded in, or adsorbed on, argon clusters have been reported by Amar *et al.* [8]. The purpose of these studies consisted, basically, in monitoring the spectroscopic properties in their evolution from those of the isolated species to those of the molecule embedded in a bulk phase.

Recently, we have published a detailed study (hereafter referred to as "paper I") on the structures and IR-spectra of the homogeneous SF_6 clusters up to the hexamer, which was based on a new site-site intermolecular potential model comprising exchange, dispersion, electrostatic, and induction terms [12]. The effective charges assigned to the atoms account for the observed vibrational transition dipole moment of the SF_6 monomer. The dispersion coefficients for the individual atomic species have been determined from the temperature dependence of the second virial coefficient of SF_6.

To calculate the IR-spectra of the found SF_6 clusters in the region of the ν_3 vibrational mode, a degenerate second order perturbation approach for frequency shifts was introduced, treating the anharmonic contributions of the intramolecular force field and the intermolecular potential as a quantum mechanical perturbation. The formalism generalizes earlier work [13,14] and was successfully used in the calculation of IR-spectra for homogeneous and mixed UF_6 clusters with Ar, as well [15,16]. The contributions to the line shifts of the SF_6 clusters have been

[a] On leave from the University of Cluj-Napoca, Department of Theoretical Physics, 3400 Cluj-Napoca, Romania.
e-mail: tbeu@phys.ubbcluj.ro

Table 1. Calculated $(SF_6)_M$ cluster structures for the energetically most stable isomers. E represents the total binding energy (in kJ/mol), and d_{SS} is the average S-S distance (in Å). Data for clusters up to the hexamer are taken from paper I.

M	E	d_{SS}	Symmetry
2	−6.68	4.90	D_{2d}
3	−18.45	5.02	D_{3d}
4	−33.90	5.18	D_2
5	−49.93	5.18	
6	−67.74	5.18	C_{4h}
7	−85.19	5.18	
8	−104.42	5.12	
9	−121.68	5.16	
10	−141.83	5.16	

analyzed and it was found that the vibrational dipole-dipole interaction is dominant. The calculated spectra compare fairly with experimental data for clusters up to the tetramer (from IR-IR double resonance experiments and IR photo-dissociation experiments with size-selected clusters) and the overall better agreement of the results obtained neglecting induction over those including it, was apparent.

The aim of the present paper is to complete the knowledge gained from the investigations reported in paper I with results concerning minimum energy structures and the corresponding IR-spectra for homogeneous $(SF_6)_M$ clusters up to the decamer and mixed $(SF_6)_2$-Ar_n clusters with up to 50 Ar atoms. The inclusion of the mixed clusters of SF_6 with Ar is necessary for a better description of our new FT-IR spectroscopy measurements on SF_6 seeded in Ar in a supersonic Laval nozzle flow. The whole body of experimental data resulted from our FT-IR studies on the clustering of SF_6 in various buffer gases (He, Ne and Ar) will be reported elsewhere [17].

In the case of the homogeneous clusters we have used the intermolecular potential of paper I including exchange, dispersion and electrostatic terms, while for the mixed clusters specific terms have been added to account for the Ar-SF_6 and Ar-Ar interactions, based on the most accurate potential models available in the literature.

In Section 2.1 we give a brief outline of our previously published perturbation approach for calculating the frequency shifts. The potential model we employ to determine the geometrical structures and line shifts of the clusters is described in Section 2.2. Section 3.1 is devoted to the description of the structures we have obtained for the homogeneous SF_6 clusters ranging from heptamer to decamer and for the mixed $(SF_6)_2$-Ar_n clusters with $n = 2 - 50$. Based on the obtained configurations, the results of our frequency shift calculations are given in Section 3.2. The results of our FT-IR spectroscopy measurements in Laval nozzle flow, as well as the comparison with the calculated spectra, are presented in Section 3.3.

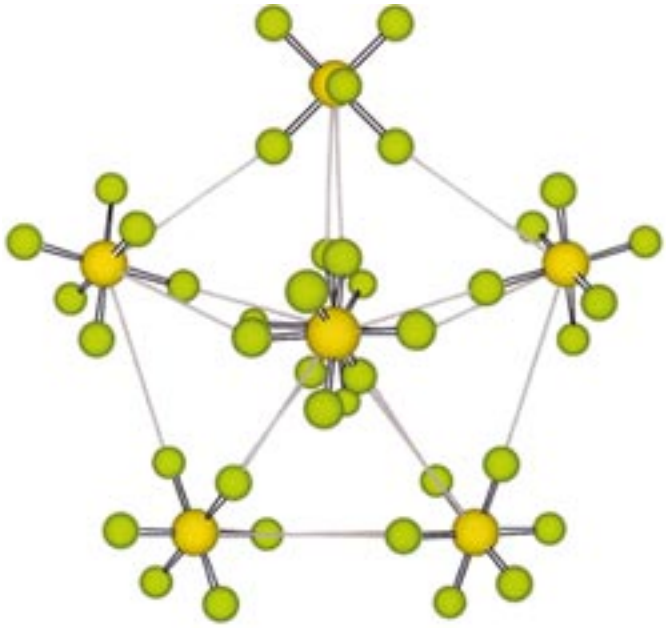

Fig. 1. Geometrical structure of the lowest energy $(SF_6)_7$ isomer.

2 Theoretical model

2.1 Frequency shift approach

For a homogeneous cluster formed of M molecules, the first-order frequency shifts $\Delta\nu_{ni}^{(1)}$ relative to a particular vibrational mode n of the monomer were shown in paper I to result by solving the eigenvalue problem

$$\sum_{n'\in\Gamma}\sum_{i'=1}^{M}\left[\frac{1}{2}\frac{\partial^2 U}{\partial q_{ni}\partial q_{n'i'}} - hc\Delta\nu_{ni}^{(1)}\delta_{nn'}\delta_{ii'}\right]c_{n'i',ni} = 0 \quad (1)$$

for $i = 1, 2, ..., M$. The perturbation matrix elements are expressed in terms of the curvature of the intermolecular potential U, which, in the case of mixed clusters, also includes the interactions with the different molecular or atomic species. q_{ni} is the position operator associated with normal mode n of molecule i. In the case of a degenerate mode, both n and n' belong to the subspace Γ of the considered normal mode, while for a non-degenerate mode, $n \equiv n'$.

The second-order line shifts can be expressed as

$$\Delta\nu_{ni}^{(2)} = \sum_{n',n''\in\Gamma}\sum_{i',i''} c_{n'i',ni}c^{*}_{n''i'',ni}\Delta\nu^{(2)}_{n'i',n''i''} ,$$

where

$$\Delta\nu^{(2)}_{n'i',n''i''} = -\frac{\delta_{i'i''}}{2hc}\sum_r \frac{1}{\omega_r}\frac{\partial U}{\partial q_{ri'}}\phi_{n'n''r}$$
$$+\frac{1}{4(hc)^2}\sum_{r\notin\Gamma}\sum_m \frac{1}{\omega_n-\omega_r}\frac{\partial^2 U}{\partial q_{n'i'}\partial q_{rm}}\frac{\partial^2 U}{\partial q_{n''i''}\partial q_{rm}}$$
$$-\frac{1}{4(hc)^2}\sum_r\sum_m \frac{1}{\omega_n+\omega_r}\frac{\partial^2 U}{\partial q_{n'i'}\partial q_{rm}}\frac{\partial^2 U}{\partial q_{n''i''}\partial q_{rm}}.$$

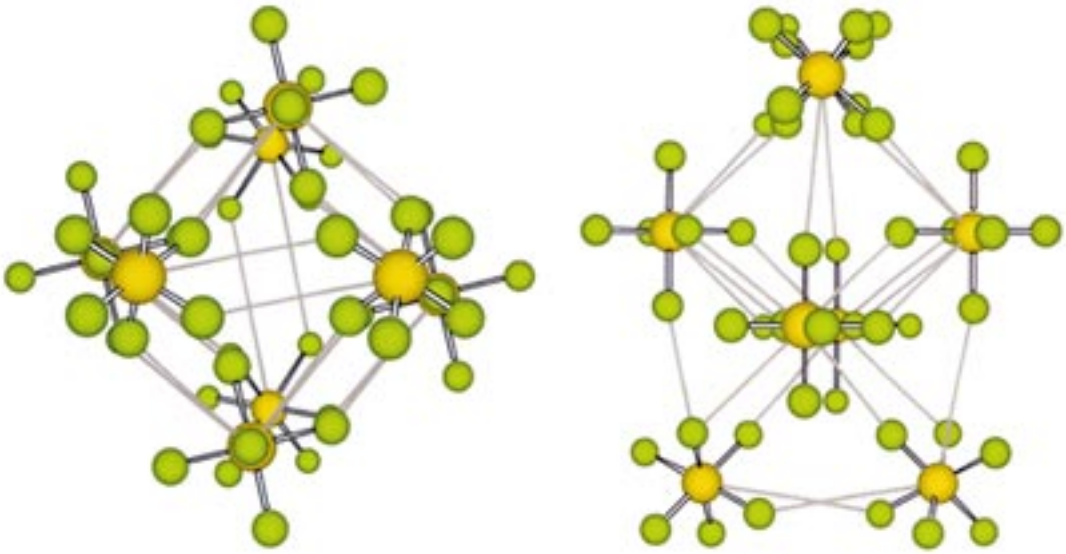

Fig. 2. Top and side view of the most stable $(SF_6)_8$ isomer.

Here ω_n and $\phi_{n'n''r}$ are harmonic frequencies and cubic force constants, respectively. The first term of $\Delta\nu^{(2)}_{n'i',n''i''}$ is expressed under a more compact (however less explicit) form, as compared to our previous publications [12,14, 15]. Obviously, the total frequency shifts are given by the sum of the first- and second-order contributions. The calculation details of the cubic force constants, $\phi_{n'n''r}$, and of the intermolecular potential derivatives with respect to the normal coordinates can be found in [12] and are based on the G-F method of Wilson [18] and the L-tensor formalism of Hoy, Mills and Strey [19].

2.2 Intermolecular potential

The SF_6-SF_6 intermolecular potential we have used for calculating the homogeneous cluster structures and the corresponding vibrational frequencies shifts is basically the one previously introduced under the name "potential I" in paper I, and it comprises exchange, dispersion, and electrostatic terms. Since the induction interaction with the polarizabilities presently available in the literature was found to be of little relevance in describing the SF_6 clusters up to the hexamer, we have no longer considered this contribution. An important feature of this site-site potential is that it depends on the relative atom positions, thus implicitly depending on the internal monomer vibrational coordinates.

In the case of the mixed $(SF_6)_2$-Ar_n clusters, we have modeled the Ar-SF_6 interaction by the anisotropic potential of Eichenauer and Le Roy [7], represented as a sum over Ar-S and Ar-F pair potentials. Explicitly, the interaction between a particular Ar atom and one of the F atoms of an SF_6 molecule, is given by

$$U_{\mathrm{Ar-F}_l}(r_l,\theta_l) = A\left[1+pP_2(\cos\theta_l)\right]e^{-br_l} - \sum_{n=3}^{5}\left[1-e^{-br_l}\sum_{k=0}^{2n}\frac{(br_l)^k}{k!}\right]\frac{C_{2n}}{r_l^{2n}}\,.$$

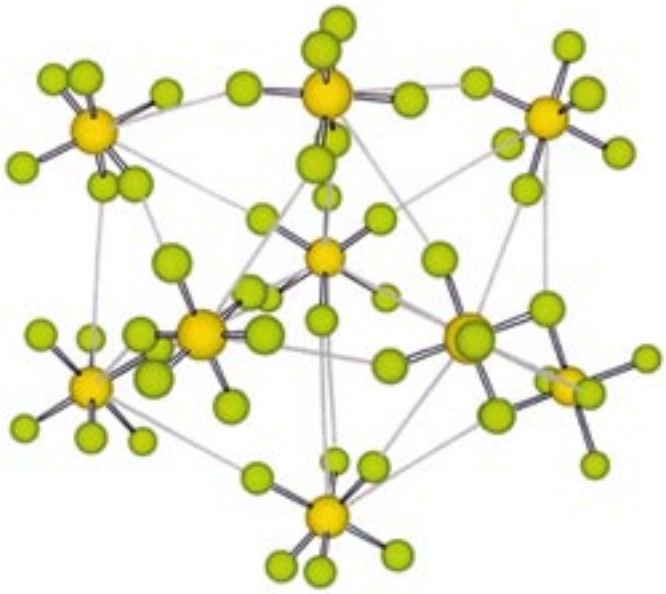

Fig. 3. Geometrical structure of the lowest energy $(SF_6)_9$ isomer.

Here $\mathbf{r}_l = \mathbf{r}_{\mathrm{Ar}} - \mathbf{r}_{\mathrm{F}_l}$ is the relative position vector of the Ar atom with respect to the F atom and θ_l is the angle subtended by vectors $\mathbf{r}_l$ and $\mathbf{r}_{\mathrm{F}_l} - \mathbf{r}_{\mathrm{S}}$ (the relative position vector of the F atom with respect to the S atom). $P_2(\cos\theta_l) = (1/2)(3\cos^2\theta_l - 1)$ is the second-order Legendre polynomial. A similar pair potential holds for the Ar-S interaction, too, except for the absence of the first term ($A = 0$) and the sole dependence on the Ar-S distance $r = |\mathbf{r}_{\mathrm{Ar}} - \mathbf{r}_{\mathrm{S}}|$.

To describe the Ar-Ar interaction, we have used the elaborate potential of Aziz and Slaman [20], which incorporates the most accurate available C_6 dispersion coefficients and was additionally fitted to the

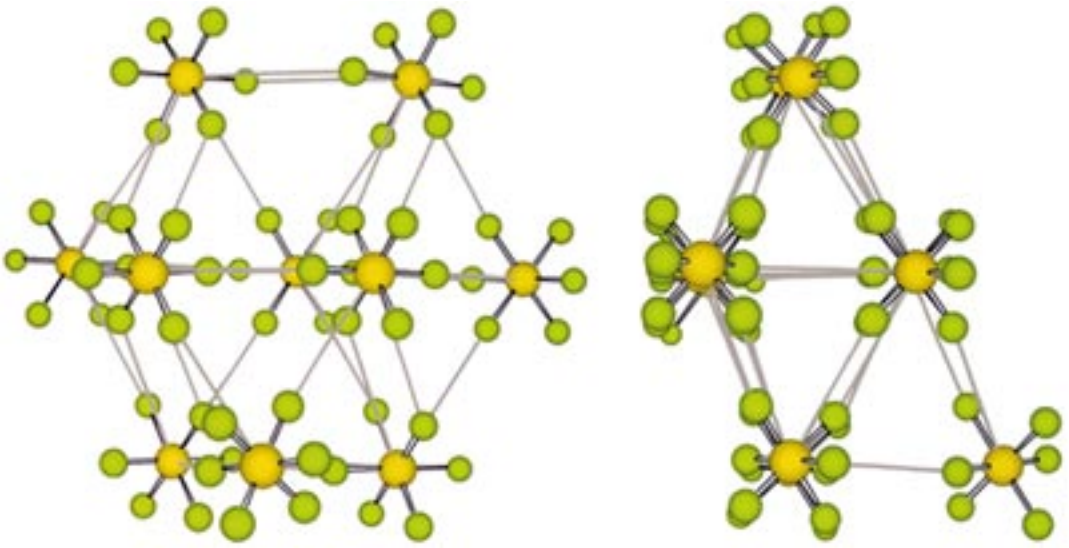

Fig. 4. Top- and side view of the most stable $(SF_6)_{10}$ isomer.

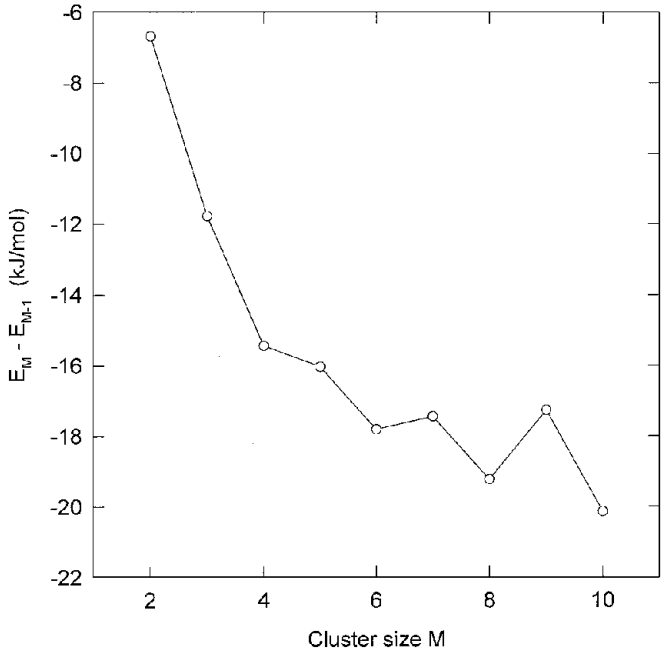

Fig. 5. Incremental binding energy of homogeneous SF_6 clusters.

experimental vibration-rotation band-system, viscosity and second virial data. The functional form of this potential is

$$U_{\mathrm{Ar-Ar}}(r) = \varepsilon A^* \exp(-\alpha^* x + \beta^* x^2) - \varepsilon F(x) \sum_{j=0}^{2} c^*_{2j+6} / x^{2j+6},$$

being expressed in terms of the dimensionless coordinate $x = r/r_m$ and with the damping function $F(x)$ defined by

$$F(x) = \begin{cases} \exp\left[-(D/x-1)^2\right], & x < D\,, \\ 1, & x \geq D\ . \end{cases}$$

All relevant data for the description of the Ar-Ar interaction can be found Table 1 of [20].

3 Results

3.1 Cluster structures

The equilibrium cluster structures have been determined by minimizing the total interaction energy of the components. More precisely, in the case of the homogeneous $(SF_6)_M$ clusters, the molecules have been considered rigid and the intermolecular potential has been minimized with respect to their relative positions, starting from randomly chosen initial configurations. The positions and orientations of the molecules have been specified by the Cartesian coordinates of their center of masses and the corresponding Euler angles, respectively. To obtain the global minimum for each cluster size M, we have performed roughly as many thousands of minimizations as given by the cluster size. In the case of the mixed $(SF_6)_2$-Ar_n clusters, the Ar positions have been treated as additional degrees of freedom, each new Ar atom being initially placed in random positions about the equilibrium structure obtained for the previous number of Ar atoms. For the mixed clusters, up to 30000 minimizations have been necessary to yield the lowest energy configurations.

Table 1 gathers the results of our structure calculations for homogeneous $(SF_6)_M$ clusters up to the decamer, in terms of the binding energy, symmetry and average distance of the nearest S atoms, d_{SS} (as a measure of the cluster "compactness"). For all cluster sizes we have listed the data for the most stable (energetically lowest) isomer. The results for the clusters up to the hexamer have been extensively discussed in paper I, where, except for the pentamer, the lowest energy configurations for all cluster sizes have been found to show remarkable symmetry properties. It was confirmed that SF_6 forms true van der Waals clusters, mainly bound by the dispersion attraction.

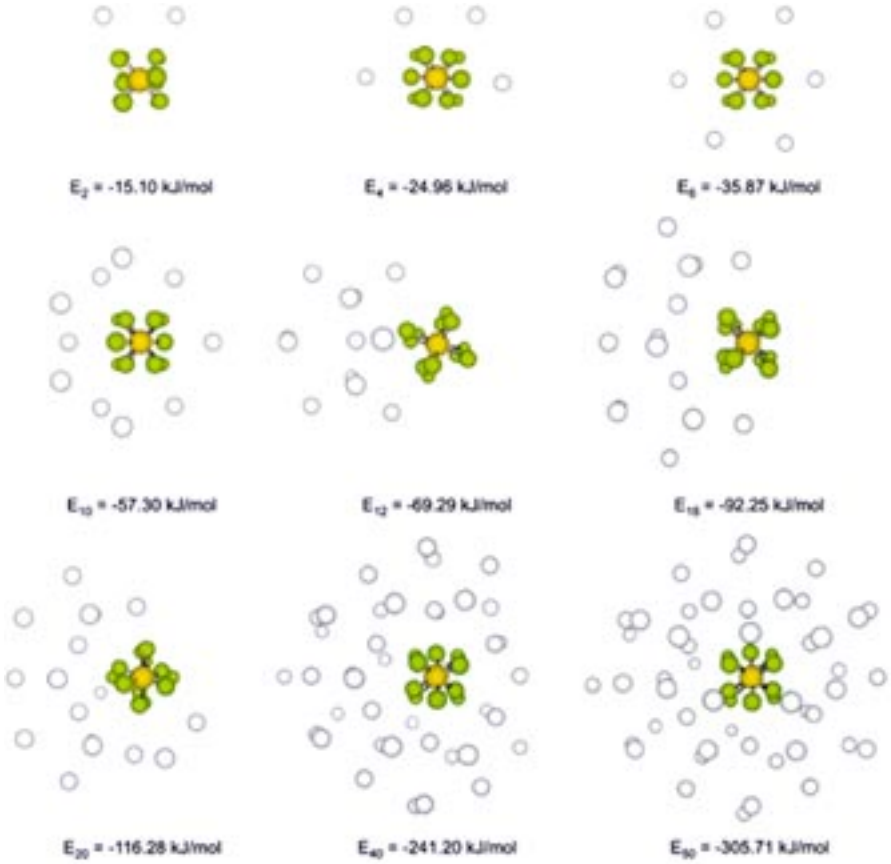

Fig. 6. Structures of the most stable $(SF_6)_2$-Ar_n clusters, for several even values of n, viewed along the SF_6-dimer axis. For each configuration, the total binding energy, E_n, is indicated.

We have depicted in Figure 1 the lowest energy heptamer. The considered isomer has a distorted bipyramidal structure with a fivefold axis, along which it is viewed. The average S-S distance preserves the value of 5.18 Å featured by the tetramer, pentamer and hexamer.

In Figure 2 a top and a side view of the energetically most stable octamer are presented. The octamer can be regarded as a superposition of two tetramer structures, as found in paper I, or, alternatively, a sequence of four reciprocally orthogonal sandwiched dimers. This very compact structure is also characterized by a smaller average d_{SS} distance as compared to the lowest energy heptamer.

The most stable nonamer (Fig. 3) has no particular symmetry, consisting of two rings and an isolated monomer in the far plane. The rings themselves consist of three and five monomers, respectively.

The lowest energy decamer, depicted as top and side view in Figure 4, exhibits a regular structure, showing the tendency to form a lattice-like arrangement of the monomers. In addition, the average S-S distance for the decamer is lower than the one for the clusters from tetramer to heptamer.

Useful information can be extracted from the plot of the incremental binding energy $E_M - E_{M-1}$ of the most stable isomers as a function of the size M (Fig. 5). The larger odd-size clusters ($M = 5, 7, 9$) show reduced energy increments relative to the previous even-size cluster. This can be correlated with their reduced symmetry and larger average d_{SS} distance and evidences the higher stability of the clusters built of "dimers". However, there is an overall saturation tendency of the incremental binding energy, meaning that, for larger clusters, each added monomer enters a host structure in which it significantly interacts only with the closest neighbors.

Since the structure calculations for the mixed clusters are extremely time consuming for the number of Ar atoms of interest, we have confined our investigations to the $(SF_6)_2$-Ar_n clusters for even values $n = 2 - 50$. We mention that the mole fraction of 0.13 used in the FT-IR experiments described in Section 3.3 approximately corresponds to $n = 15$. The obtained cluster structures, along with the corresponding binding energies, are depicted in Figure 6 for some selected values of n. All structures are viewed along the SF_6 "dimer" axis. It should be noted that the configurations with n up to 10 tend to form a hexagonal ring transverse to the SF_6 dimer axis. Starting with $n = 12$, however, this trend is abandoned, and an energetically more favorable cell-like structure is developed up to $n = 50$, with the Ar atoms forming closed shells about the SF_6 dimer axis.

The binding energy E_n of the most stable $(SF_6)_2$-Ar_n isomers decreases in a smooth manner with the number

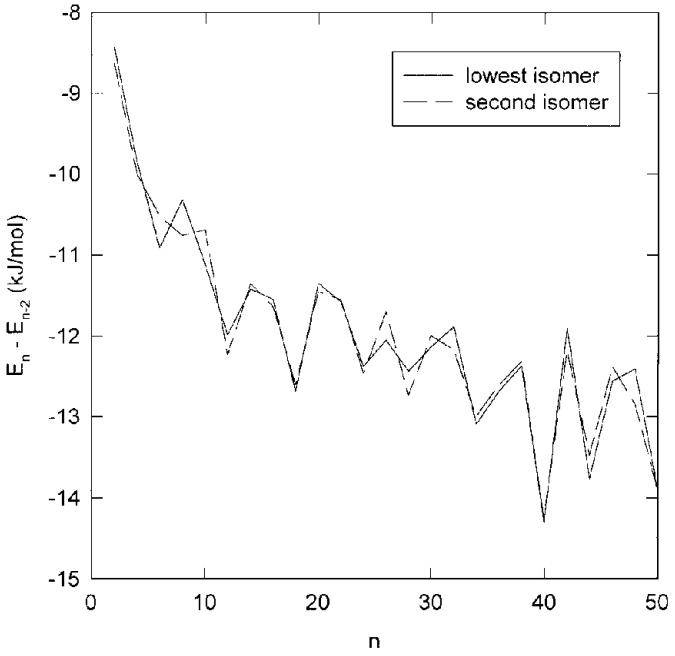

Fig. 7. Incremental binding energy of the lowest and second lowest energy configurations of the $(SF_6)_2$-Ar_n clusters.

of Ar atoms n. The plot of the corresponding incremental binding energies is depicted in Figure 7. We have defined the incremental binding energy as $E_n - E_{n-2}$, since we have considered only even values for n in our calculations. The saturation tendency of the overall decreasing behavior becomes apparent for higher number of Ar atoms. The oscillating plot corresponding to the most stable isomers is closely followed by the one for the second lowest isomers and this is a result of the quasi-continuum of stable isomer states (with slightly different positions of the Ar atoms) in the vicinity of the most stable configuration.

3.2 Frequency shifts

In our band shift calculations for both homogeneous and mixed SF_6 clusters, we have focused on the fundamental excitation of the ν_3 vibrational mode of the SF_6 monomer at 947.968 cm^{-1}.

As discussed in paper I, the interaction of the monomers within the clusters causes the ν_3 vibration to be split up into redshifted parallel bands ($\parallel$) and blueshifted perpendicular bands ($\perp$). Due to the threefold degeneracy of the ν_3 mode, in the dimer spectrum, for example, up to six lines may be observed if the symmetry is sufficiently perturbed. For the most stable dimer, however, as a consequence of its D_{2d} symmetry, only two lines appear (see the lowest panel of Figure 8): one redshifted line ($\parallel$), associated with a vibration mainly taking place along the dimer symmetry axis, and a doubly degenerate blueshifted line ($\perp$), corresponding to a transverse vibration. For the higher clusters, the parallel or perpendicular character of a band is rather related to the main symmetry axis.

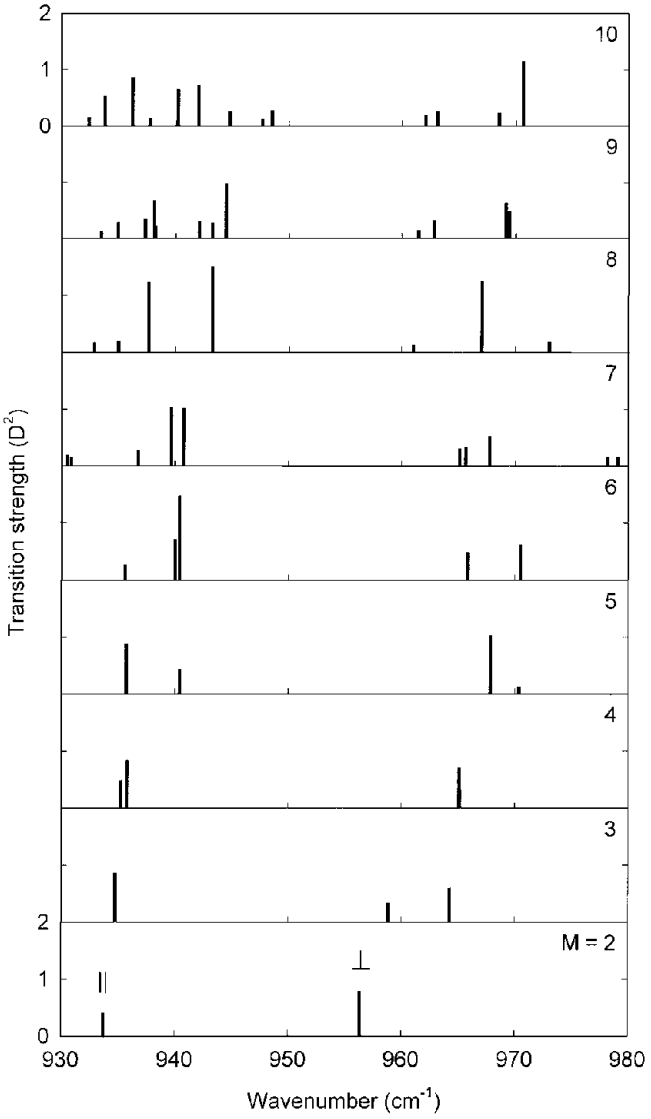

Fig. 8. Calculated stick spectra of homogeneous SF_6 clusters from dimer to decamer. For all cluster sizes, the most stable isomer is being considered.

The second-order line shifts for the SF_6 clusters typically amount to less than 0.5 cm^{-1} and their reduced magnitude has turned out to be a consequence of the reduced anharmonicity of the monomer vibrations and of the small intermolecular potential curvature in the vicinity of the global minimum, as well.

The interaction mechanism which was found to be mainly responsible for the frequency shifts, is the vibrational dipole-dipole interaction, while the effects of the exchange and dispersion couplings have proved to be completely negligible, even though they are determining for the geometrical cluster structures [12].

As was discussed in detail in paper I, the calculated stick spectra of the homogeneous SF_6 clusters up to the tetramer agree very well with the results of the two most recently reported sets of measurements with size-selection techniques: the IR-IR double-resonance experiments of

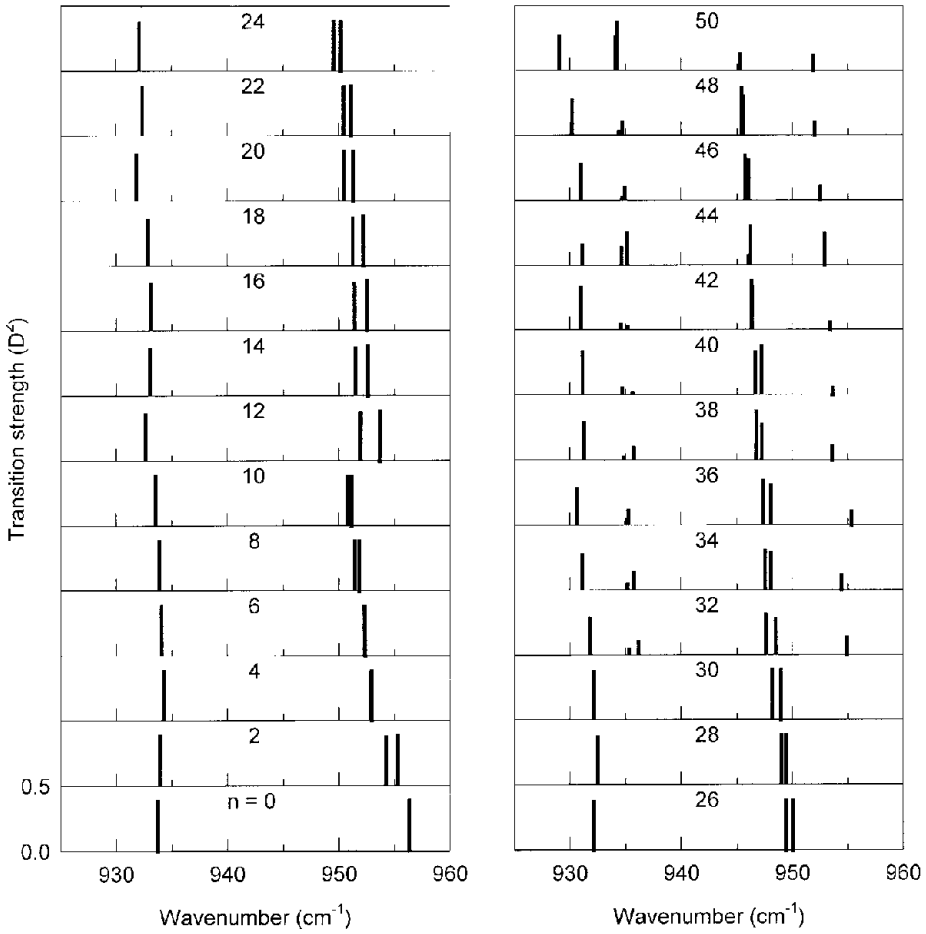

Fig. 9. Calculated stick spectra of $(SF_6)_2$-Ar_n clusters. For all cluster sizes, the most stable isomer is being considered.

Heijmen *et al.* [4], and the vibrational predissociation experiments of Huisken *et al.* [3]. Unfortunately, no size-selected observed data for clusters higher than tetramer are available.

Figure 8 shows the stick spectra of the SF_6 clusters up to the decamer. The lines have been denoted according to the sign of the frequency shift: with $\parallel$ for redshifted lines and with $\perp$ for the blueshifted ones. While the "parallel" lines tend to preserve the red boundary of the spectra at about 935 cm^{-1} with increasing cluster size, the "perpendicular" lines gradually move toward higher frequencies, however with a saturation tendency, which brings about an almost non-varying average splitting from pentamer to decamer of about 35 cm^{-1}. Whereas in the case of the clusters up to the hexamer the splitting pattern remains quite simple, from the heptamer onward, the lack of a well-defined geometrical symmetry and the increase of the number of SF_6 monomers in non-equivalent positions causes the stick spectra to be much less structured. With its three clearly individualized lines (the others being of much smaller intensity), the octamer appears to be an exception to some extent. This is obviously a consequence of its more compact and regular structure, as was discussed in the previous section.

The stick spectra of the mixed $(SF_6)_2$-Ar_n clusters, depicted in Figure 9 for $n = 2 - 50$, show a behavior just opposed to the spectra for the homogeneous clusters: with increasing cluster size, the lines are systematically redshifted. However, when going from $n = 10$ to $n = 12$ there is a change in scenario and the discontinuity in the evolution of the spectral lines can be correlated with the abrupt change of geometrical structure of $(SF_6)_2$-Ar_{12} as compared to its predecessors. An interesting finding is that the total splitting for the $(SF_6)_2$-Ar_{50} cluster (22.84 cm^{-1}) is almost the same as for $(SF_6)_2$ (22.64 cm^{-1}), even though the lines of the former are redshifted by approximately 5 cm^{-1}. This indicates that the splitting is mainly due to the dimer, while the supplementary redshift is caused by the surrounding Ar atoms.

3.3 FT-IR spectra of SF_6 in a supersonic Laval nozzle flow

We have investigated the clustering of SF_6 seeded in Ar in a continuous Laval nozzle flow and, particularly, the clustering onset conditions by measuring the FT-IR spectra of the SF_6 monomer and clusters in the nozzle. The experimental techniques have been previously employed in our

studies on the FT-IR spectroscopy of the UF_6 clustering and the experimental setup (including the Laval nozzle) is basically the same [21,22].

Barnes and Gough performed FT-IR measurements in supersonic free jets to observe the spectra of SF_6 clusters [23]. As they pointed out, FT-IR spectroscopy has the advantage that a very wide spectral coverage can be obtained, superior to that of any laser system, and all transitions can be recorded in the spectrum at the same time. In the conventional supersonic free jet used by Barnes and Gough, however, it was impossible to determine the density of the molecules accurately because the jet divergence was large and the density was not uniform. By contrast, in a continuous supersonic Laval nozzle flow, the density is uniform in the direction perpendicular to the flow and the nozzle can be designed so as to give an appropriate divergence angle. Furthermore, the local pressure can be measured with a conventional manometer attached to the nozzle.

Hence, FT-IR spectroscopy with continuous supersonic Laval nozzle flow is most suited for simultaneous observation of the spectra of both the monomer and clusters and we have determined by this method the clustering onset temperature and density of SF_6. The detailed discussion of our FT-IR measurements on the clustering of SF_6 in various buffer gases (He, Ne and Ar) will be reported elsewhere [17], and we will present in what follows only the results of our FT-IR spectroscopy studies on SF_6 seeded in Ar.

We measured the IR spectra of SF_6 gas at a mole fraction of 0.13 in Ar at six equidistant positions between 15 and 40 mm downstream from the Laval nozzle throat, which is 1.2 mm wide. The obtained spectra are shown in Figure 10. All spectra clearly feature the P-, Q- and R-branches of the $^{32}SF_6$ monomer in the range between 940 and 960 cm^{-1}. Calculations evidence that the small peak around 930 cm^{-1}, visible in the spectrum obtained at 15 mm from the nozzle throat, is due to the $^{34}SF_6$ monomer and the even smaller peak around 940 cm^{-1} is to be attributed to $^{33}SF_6$.

The additional peak developing around 942 cm^{-1}, which dominates the spectrum for positions beyond 30 mm downstream from the Laval nozzle throat, is obviously due to homogeneous SF_6 clusters. This can be easily explained by inspecting Figure 11, which shows in the upper panel the FT-IR spectrum obtained at 30 mm downstream from the nozzle throat (corresponding to a total pressure of 9.21 Torr) and gathers the calculated stick spectra of the homogeneous SF_6 clusters up to the decamer in the middle panel. Except for the dimer, the perpendicular blueshifted lines of all cluster sizes contribute to the broad and flat peak located between 960 and 970 cm^{-1}.

However, the smooth compact shoulders of the spectrum in the ranges 920-940 cm^{-1} and 950-960 cm^{-1} can no longer be explained by the presence of homogeneous SF_6 clusters alone. Even extrapolating to larger sizes the trend found for the homogeneous clusters, only dispersed lines of quite low intensity are expected to result in the considered regions. On the other hand, the calculated spectra

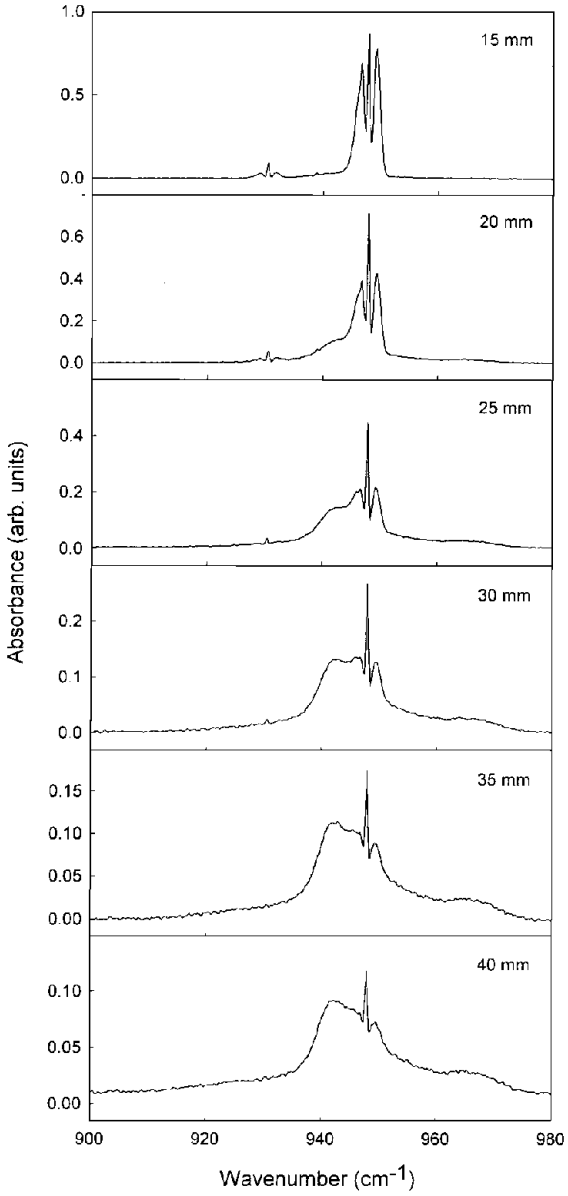

Fig. 10. FT-IR spectra of SF_6 at a mole fraction of 0.13 in Ar obtained at six different positions downstream from the Laval nozzle throat.

of the less stable isomers do not emphasize significant differences, which could possibly lead to qualitatively different conclusions. The only plausible explanation is offered by the continuum of lines due to the mixed clusters of SF_6 with Ar. The lower panel of Figure 11 displays the stick spectra of the $(SF_6)_2$-Ar_n clusters. Since the spectral lines corresponding to the higher number of Ar atoms are shifted to the left of each of the two groups, the lines for $n > 50$ are expected to continue this trend and to extend toward lower wave numbers. Moreover, this behavior is likely to characterize also the mixed clusters consisting of more than two SF_6 monomers.

As part of their solvation studies, Amar *et al.* (see Fig. 1 of [8]) have measured both conventional coexpansion

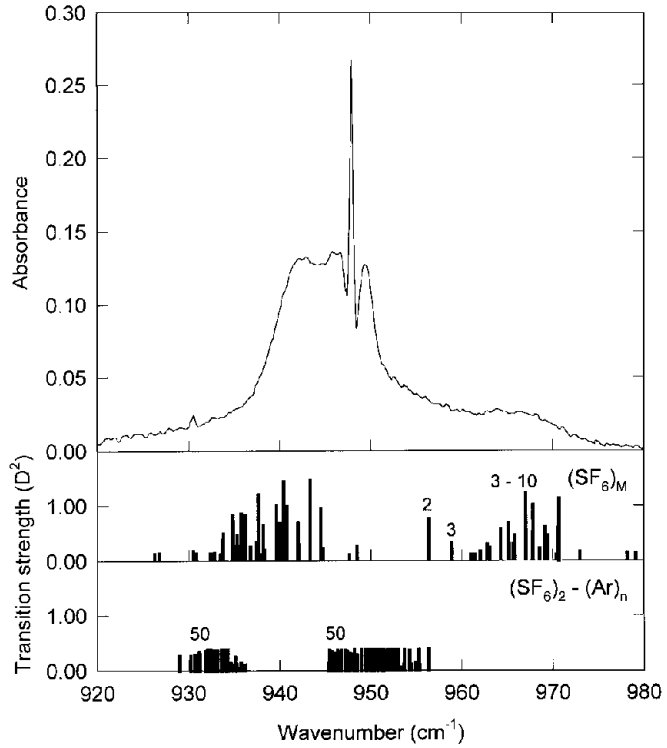

Fig. 11. FT-IR spectrum of SF_6 clusters seeded in Ar obtained at 30 mm downstream from the Laval nozzle throat and calculated stick spectra of $(SF_6)_{2\text{-}10}$ and $(SF_6)_2$-$Ar_{2\text{-}50}$ clusters.

spectra and pick-up spectra of SF_6-Ar_n clusters in the range between 935 and 949 cm^{-1}, roughly covering the region between the two groups of $(SF_6)_2$-Ar_n lines calculated in this work. The SF_6-Ar_n spectra are dominated by the band located at ∼938 cm^{-1}, which was attributed to the ν_3 vibration of SF_6 residing in matrix-like sites in solid argon clusters [6]. This band is visible as a very low intensity peak in our FT-IR spectra up to 20 mm downstream from the Laval nozzle throat. Beyond this position it is completely dominated by the major band developing around 942 cm^{-1} due to the homogeneous SF_6 clusters. Since the bulk absorption frequency (∼938 cm^{-1}) determines the left boundary of the SF_6-Ar_n spectrum, while the right boundary is obviously the SF_6 monomer frequency, there is no overlap between the SF_6-Ar_n bands and the spectrum calculated for the $(SF_6)_2$-Ar_n clusters.

The band occurring in the pick-up spectra of Amar *et al.* around 941 cm^{-1} indicates that the environment of the SF_6 molecules responsible for this band involves interactions with fewer Ar atoms than required to fully solvate the chromophore. Since in pick-up experiments, the chromophore is attached to the cluster surface, this band has been assigned to species in which the SF_6 is located at the cluster surface. The results of Amar *et al.* suggest that at lower stagnation pressures, or for smaller cluster sizes ($n \leq 60$), the SF_6 molecule prefers to be located *inside* the argon clusters. A similar behavior was evidenced in Section 3.1 for the $(SF_6)_2$-Ar_n clusters, too, with the Ar atoms forming closed shells about the SF_6 dimer axis.

The results of the Monte Carlo simulations of Eichenauer *et al.* [7] are consistent with the measurements of Amar *et al.* The lines corresponding to the SF_6-Ar_n clusters are again located in the gap between our two groups of $(SF_6)_2$-Ar_n lines, being monotonically redshifted with respect to the ν_3 peak of the SF_6 monomer with increasing Ar atom number. For example, the frequency shift for 50 Ar atoms amounts to approximately -5.8 cm^{-1} and for 100 Ar atoms, to -6.7 cm^{-1}. However, due to their lower intensity as compared to that of the homogeneous clusters, these lines cannot be discriminated in the observed FT-IR spectrum.

4 Conclusions

The present study completes the investigations initiated in paper I, regarding the structure and IR-spectra of homogeneous and mixed clusters involving SF_6 molecules. While the $(SF_6)_M$ clusters up to the hexamer have been extensively analyzed in paper I, the new results refer to the homogeneous clusters from heptamer to decamer and to the mixed $(SF_6)_2$-Ar_n clusters.

In all calculations concerning the higher homogeneous clusters, the site-site intermolecular potential for SF_6 developed in paper I has been used. The average S-S distance of these clusters and the incremental binding energy have been employed to correlate the "compactness" of the found minimum energy structures with their symmetry properties. Whereas the clusters up to the hexamer exhibit clearly defined symmetries, the larger ones generally lack such properties. Quite surprisingly, already the decamer shows rudiments of a solidlike structure. The larger incremental binding energies of the clusters composed of an even number of monomers suggest a higher stability of these as compared to those composed of an odd number of molecules. It is confirmed that SF_6 forms true van der Waals clusters, mainly bound by the dispersion attraction, the effect of the induction interactions being negligible.

Based on the SF_6-SF_6 intermolecular potential, by adding appropriate terms for the Ar-SF_6 and Ar-Ar interactions, an accurate potential energy surface for the mixed $(SF_6)_2$-Ar_n clusters has been built. The configurations with n up to 10 tend to form a hexagonal ring transverse to the SF_6 dimer axis. Starting with $n = 12$, however, an energetically more favorable cell-like structure is formed, which is continued up to $n = 50$.

The degenerate second-order perturbation formalism introduced in paper I is used to calculate the IR-spectra of the found SF_6 clusters (both homogeneous and mixed) in the region of the ν_3 vibrational mode. Although much smaller than the first-order frequency shifts, the second-order ones accomplish a fine-tuning of the calculated spectra. Among the contributions to the line shifts, those attributed to the vibrational dipole-dipole interaction are found to be dominant.

The calculated spectra compare fairly with the available experimental data for homogeneous clusters up to

the tetramer. To explain our recent FT-IR spectroscopy measurements on SF_6 seeded in Ar, however, besides the spectra of the homogeneous clusters, which account for the two peaks observed around 942 and 965 cm^{-1}, the spectra of the mixed $(SF_6)_2$-Ar_n clusters have to be considered, as well. The smooth shoulders of the spectrum in the ranges 920-940 cm^{-1} and 950-960 cm^{-1} can be attributed to the continuum of lines due to the mixed clusters of SF_6 with Ar.

References

1. J. Geraedts, S. Stolte, J. Reuss, Z. Phys. A **304**, 167 (1982); J. Geraedts, M. Waayer, S. Stolte, J. Reuss, Faraday Discuss. Chem. Soc. **73**, 375 (1982).
2. M. Snels, R. Fantoni, Chem. Phys. **109**, 67 (1986); M. Snels, J. Reuss, Chem. Phys. Lett. **140**, 543 (1987).
3. F. Huisken, M. Stemmler, Chem. Phys. **132**, 351 (1989).
4. B. Heijmen, A. Bizzarri, S. Stolte, J. Reuss, Chem. Phys. **132**, 331 (1989).
5. T.E. Gough, D.G. Knight, G. Scoles, Chem. Phys. Lett. **97**, 155 (1983).
6. T.E. Gough, D.G. Knight, P.A. Rowntree, G. Scoles, J. Phys. Chem. **90**, 4026 (1986).
7. D. Eichenaueer, R.J. Le Roy, J. Chem. Phys. **88**, 2898 (1988).
8. F.G. Amar, S. Goyal, D.J. Lavandier, L.Perera, G. Scoles in *Clusters of Atoms and Molecules II*, Ed. H. Haberland, Springer Verlag, Berlin, 1994, p. 19.
9. J.W.I. van Bladel, A. van der Avoird, J. Chem. Phys. **92**, 2837 (1989).
10. A. Boutin, J.-B. Maillet, A.H. Fuchs, J. Chem. Phys. **99**, 9944 (1993); A. Boutin, B. Rousseau, A.H. Fuchs, Chem. Phys. Lett. **218**, 122 (1994).
11. U. Buck, H. Meyer, Phys. Rev. Lett. **52**, 109 (1984).
12. T.A. Beu, K. Takeuchi, J. Chem. Phys. **103**, 6394 (1995).
13. U. Buck, B. Schmidt, J. Chem. Phys. **98**, 9410 (1993).
14. T.A. Beu, Z. Phys. D **31**, 95 (1994).
15. T.A. Beu, J. Onoe, K. Takeuchi, J. Chem. Phys. **106**, 5910 (1997).
16. T.A. Beu, J. Onoe, K. Takeuchi, J. Chem. Phys. **109**, 8295 (1998).
17. Y. Okada, T.A. Beu, K. Takeuchi, to be published.
18. E.B. Wilson, J.C. Decius, P.C. Cross, *Molecular Vibrations* (McGraw-Hill, New York, 1955).
19. A.R. Hoy, I.M. Mills, G. Strey, Mol. Phys. **24**, 1265 (1972).
20. R.A. Aziz, M.J. Slaman, Molec. Phys. **58**, 679 (1986).
21. S. Tanimura, Y. Okada, K. Takeuchi, J. Phys. Chem. **100**, 2842 (1996).
22. Y. Okada, S. Tanimura, H. Okamura, A. Suda, H. Tashiro, K. Takeuchi, J. Molec. Struct. **410-411**, 299 (1997).
23. J.A. Barnes, T.E. Gough, Chem. Phys. Lett. **130**, 297 (1986).